Title

Corrigendum to “Zircon solubility and zirconium complexation in H2O+Na2O+SiO2±Al2O3 fluids at high pressure and temperature” [Earth Planet. Sci. Lett. 349–350 (2012) 15–25]

Authors

Wilke, Max
Schmidt, Christian
Dubrail, Julien
et al.

Publication Date

2013-07-01

DOI

10.1016/j.epsl.2013.04.010

Peer reviewed

Earth and Planetary Science Letters 349–350 (2012) 15–25

Contents lists available at SciVerse ScienceDirect

Earth and Planetary Science Letters

journal homepage: www.elsevier.com/locate/epsl

Letters

Zircon solubility and zirconium complexation in $H_2O+Na_2O+SiO_2\pm Al_2O_3$ fluids at high pressure and temperature

Max Wilke [a,*], Christian Schmidt [a], Julien Dubrail [a], Karen Appel [b], Manuela Borchert [b], Kristina Kvashnina [c], Craig E. Manning [d]

[a] Deutsches GeoForschungsZentrum (GFZ), Telegrafenberg, 14473 Potsdam, Germany
[b] Deutsches Elektronen Synchrotron, Notkestr. 85, 22607 Hamburg, Germany
[c] European Synchrotron Radiation Facility, 6 rue Horowitz, 38043 Grenoble, France
[d] Department of Earth and Space Sciences, University of California, Los Angeles, CA 90025-1567, USA

ARTICLE INFO

Article history:
Received 9 April 2012
Received in revised form
25 June 2012
Accepted 27 June 2012
Editor: T.M. Harrison

Keywords:
subduction zone fluids
high-field strength elements
X-ray spectroscopy

ABSTRACT

Zircon is an important host mineral for many high-field strength elements (HFSE), particularly Zr and Hf. Thus, its solubility in geologic fluids at high pressure and temperature plays an important role in terrestrial cycling of these elements during processes in the Earth's crust and mantle. We performed in-situ high-pressure, high-temperature measurements of zircon solubility in H_2O–$Na_2Si_3O_7$, H_2O–$Na_2Si_3O_7+Al_2O_3$, H_2O–$Na_2Si_2O_5$, H_2O–$NaAlSi_3O_8$ fluids, as well as of baddeleyite solubility in H_2O–NaOH fluids, by in-situ synchrotron radiation X-ray fluorescence analysis using hydrothermal diamond-anvil cells. Zirconium complexation in fluids in equilibrium with zircon was constrained by in-situ X-ray absorption near-edge structure (XANES) spectroscopy. Zircon solubility is strongly enhanced by addition of $Na_2Si_3O_7$ to H_2O. The degree of enhancement increases with $Na_2Si_3O_7$ concentration. The Zr content of fluids containing 10 wt% $Na_2Si_3O_7$ reached up to 86 ± 2 ppm Zr at 550 °C and 400 MPa. At 30 wt% $Na_2Si_3O_7$, the maximum Zr concentration was 997 ± 6 ppm at 600 °C and 440 MPa. Zircon solubility in these fluids decreases considerably with pressure and increases slightly with temperature. Addition of Al_2O_3 decreases the zircon solubility. In H_2O–$NaAlSi_3O_8$ fluids, the Zr concentrations are in the sub-ppm to ppm range. Zr concentrations in NaOH solutions in equilibrium with baddeleyite reached up to 390 ± 2 ppm at 600 °C and 930 MPa and increase with pressure and temperature. In-situ XANES spectra collected on Zr in H_2O–$Na_2Si_3O_7$, H_2O–$Na_2Si_3O_7+Al_2O_3$, H_2O–NaOH, and H_2O–HCl fluids in equilibrium with zircon provide evidence for strong differences in the Zr complexation between these fluids. Comparison of XANES spectra to those of model compounds and ab-initio simulation of XANES spectra revealed $^{[8]}$Zr for the HCl solution, $^{[7]}$Zr for the NaOH solution, and $^{[6]}$Zr for the Na–Al-silicate-bearing solutions. For the latter solutions, formation of alkali zircono-silicate complexes is indicated by the strong dependence of zircon solubility on Na/Al and the similarity of the XANES spectra to spectra simulated based on the local structure around Zr in the alkali zircono-silicates vlasovite and catapleite. Alkali zircono-silicate complexes are responsible for the enhancement of Zr concentrations in Na–Al-silicate-bearing solutions and very likely play an important role for mobilization of HFSE during fluid–rock interaction. Because high alkali/Al can be expected in aqueous fluids at high pressure and temperature due to incongruent dissolution of feldspar and mica, the increase of zircon solubility along the $NaAlSi_3O_8$–$Na_2Si_3O_7$ join points to potentially considerable Zr or HFSE transport by silicate-bearing aqueous fluids in the lower crust and upper mantle.

1. Introduction

The mobilization of elements within subduction zones and the formation of magmas play a major role in the evolution of the Earth's crust and upper mantle. Differential mobilization of elements leads to the characteristic depletion of high-field-strength elements (HFSE, i.e., Ti, Zr, Hf, Nb and Ta) relative to large-ion-lithophile elements (LILE, i.e., Rb, Sr, Cs, Ba, Pb, U and Th) in primitive arc magmas with respect to mid-ocean ridge basalt (e.g. Perfit et al., 1980; McCulloch and Gamble, 1991; Elliott et al., 1997). This characteristic trace element concentration pattern contains information on the genesis of these magmas in subduction zone settings. Therefore, HFSE are unique tracers of this large-scale mass and energy transfer process in the Earth's interior.

* Corresponding author.
E-mail address: max@gfz-potsdam.de (M. Wilke).

0012-821X/$ - see front matter © 2012 Elsevier B.V. All rights reserved.
http://dx.doi.org/10.1016/j.epsl.2012.06.054

Despite their importance as geochemical tracers, the mechanism that causes the HFSE depletion is still not completely understood. The HFSE depletion is typically assigned to the preferential mobilization of LILE by aqueous fluids released from the downgoing slab. HFSE strongly partition into accessory phases like rutile or zircon. Both are common accessory minerals found in many lithologies over a wide pressure and temperature range (e.g. Philippot and Selverstone, 1991; Van Baalen, 1993; Brenan et al., 1994; Hoskin and Schaltegger, 2003). Thus, these accessory phases play a central role in controlling the distribution of HFSE during metamorphism and partial melting in orogenic cycles (Kamber and Collerson, 2000; Rudnick et al., 2000). For example, fluid–rock interaction leads to retention of HFSE in metamorphic rutile or zircon and could eventually be responsible for HFSE-depleted arc magmas. This model is based on the view that the solubility of these minerals is quite low in assumed compositions of subduction zone fluids. Recently it has been shown that the solubility of rutile in pure H_2O is indeed low even at high pressures and temperatures (Tropper and Manning, 2005; Audétat and Keppler, 2005). In the case of zirconium compounds, the solubility of Zr in H_2O is lower by orders of magnitude (e.g. Tole, 1985; Newton et al., 2005, 2010). However, many field observations indicate that the assumption of immobility is not always valid. It is known that Ti-minerals such as titanite, rutile, brookite, anatase, and ilmenite in alpine clefts in metamorphic rocks are of hydrothermal origin, and that fluids can mobilize and transport significant amounts of Ti over long distances at eclogite-facies conditions (e.g., Philippot and Selverstone, 1991; John et al., 2008). Similarly, zircon grains found in natural examples may show textures/structures indicating significant dissolution and subsequent overgrowth of zircon (e.g. Liati and Gebauer, 1999; Möller et al., 2002; Vavra et al., 1996). Dempster et al. (2004) even found outgrowth rims and newly crystallized fine-grained zircon formed in slates at temperatures below 350 °C.

In the case of Ti, enhanced rutile solubility has been observed in the presence of complexing agents in the fluid, including Cl^- or F^- (Rapp et al., 2010), and aluminosilicate components in aqueous solution (Manning et al., 2008; Antignano and Manning, 2008; Hayden and Manning, 2011). Addition of 10 wt% albite component, $NaAlSi_3O_8$, increases the solubility of rutile by one to two orders of magnitude (Audétat and Keppler, 2005; Antignano and Manning, 2008). Moreover, the studies of Antignano and Manning (2008) and Hayden and Manning (2011) reveal systematic increases in rutile solubility with increasing concentration of dissolved albite in H_2O. The authors suggested that complexing of Ti (and by extrapolation of all HFSE) with dissolved silicate components, that could be provided by the silicate components derived from surrounding lithologies, would be an efficient mechanism to promote HFSE mobility and transport during fluid–rock interaction.

There are even fewer studies of Zr in geological fluids. Substantial Zr concentrations in equilibrium with zircon are reported for acidic or basic solutions at relatively low temperatures and pressure (Ewing et al., 1982; Tole, 1985; Schmidt et al., 2006). Zircon solubility in chloride fluids at high pressure and temperature was found to be moderate (Ayers and Watson, 1991), although the methods used significantly overestimated solubility (Tropper and Manning, 2005; Antignano and Manning, 2008). Regardless, Zr concentrations in hydrous silicate melts in equilibrium with zircon are substantial even at relatively low temperatures (700–1020 °C; Watson, 1979; Watson and Harrison, 1983). This suggests that zircon solubility may rise significantly with Na–Al silicate components, as is the case for rutile (Antignano and Manning, 2008; Hayden and Manning, 2011).

If HFSE solubilities in H_2O depend strongly on the concentration and composition of dissolved Na–Al silicates, then it is important to understand not only compositional dependences, but also the nature of complexing and coordination in the fluid phase. Unfortunately, Na–Al silicates dissolved in H_2O form a wide range of solute complexes (e.g., Tanaka and Takahashi, 1999; Mysen and Takahashi, 2010). In addition, there is only fragmentary knowledge on the structure of the complexes of HFSE in aqueous silicate-bearing fluids at conditions of the lower crust and the upper mantle. The very low concentrations of HFSE in aqueous fluids present severe experimental challenges for acquiring spectroscopic data on these systems. Although Manning et al. (2008) were able to obtain X-ray fluorescence (XRF) spectra of titanium at in-situ conditions with a diamond anvil cell, the strong absorption of X-rays by diamond at the energy of the Ti K-edge hinders in-situ X-ray absorption spectroscopy on Ti in the fluid with this apparatus.

In this study, we use synchrotron radiation XRF analysis and hydrothermal diamond anvil cells to obtain zircon solubility data over a wide pressure and temperature range for fluids containing Na–Al silicate or NaOH components. X-ray absorption near-edge structure (XANES) at the Zr K-edge was applied to constrain the Zr complexation mechanism in the fluids. The high X-ray energy (17,998 eV) means that absorption of X-rays by the diamond is low. Structural models of the local environment of elements in the fluids were derived by comparing experimental XANES spectra to ab initio simulations using the multiple-scattering FEFF software package (Rehr and Albers, 2000; Rehr et al., 2008). By combining the first in-situ zircon solubility data and XANES spectra, we will show that Na–Al silicate components in the fluid are of critical importance for enhancing Zr concentrations in aqueous fluids by formation of alkali zircono-silicate complexes. The results obtained in this study imply that the fluid composition resulting from chemical interaction with the surrounding rock matrix will have substantial influence on the mobility of HFSE during metamorphic processes such as those found in subduction zone settings.

2. Experimental

2.1. High-pressure setup, fluid compositions and starting materials

High pressure–high temperature in-situ experiments were performed using modified Bassett-type hydrothermal diamond-anvil cells (HDAC) optimized for X-ray absorption and X-ray ray fluorescence measurements. Detailed descriptions of the HDAC are given in Bassett et al. (1993), Schmidt and Rickers (2003), Schmidt et al. (2007), Manning et al. (2008), Borchert et al. (2009) and Wilke et al. (2010). Briefly, the initial assemblage in the sample chamber at ambient conditions consisted of solid starting materials (zircon crystals ± glass), an aqueous liquid and a vapor bubble. In this study, the fluid composition was varied by adding various amounts of silicate components to the fluid or by using NaOH or HCl solutions. Na and Na–Al silicate components were placed in the sample chamber as pieces of glass with precisely determined dimensions using a microscope scale. The glass pieces dissolved in the aqueous fluid at high pressure and temperature. The concentration of the added components was calculated from the dimensions of the glass piece assuming a density of 2.4 g/cm^3 for NS3, NS3Al5, NS3Al1, albite and 2.5 g/cm^3 for NS2 (see below for abbreviations, Mazurin et al., 1983, 1987), the density of the aqueous fluid and the volume of the sample chamber. The uncertainties in the concentration of the added glass components are about 10%.

Five glass compositions were used as starting material: $Na_2Si_3O_7$ (NS3), $Na_2Si_2O_5$ (NS2), $Na_2Si_3O_7+1$ wt% Al_2O_3 (NS3Al1), $Na_2Si_3O_7+5$ wt% Al_2O_3 (NS3Al5), and $NaAlSi_3O_8$ (albite). The glasses were synthesized from oxides and carbonates at 1600 °C

(albite) and 1300 °C (other compositions). Composition and homogeneity of the glasses was checked using electron beam microanalysis on polished sections and ICP-OES analysis after dissolution of glass pieces in acid. Zircon crystals were synthesized in a 1 atm furnace from oxide mixtures, zircon seeds, and lead flux in a Pt capsule using a temperature ramp from 1430 to 1350 °C at 1 °C/h with subsequent quench, followed by treatment with 48% hydrofluoric acid to remove excess glass. The mean composition determined by electron microprobe is (wt%) SiO_2 32.73 ± 0.36, HfO_2 1.48 ± 0.31, ZrO_2 66.40 ± 0.28 (46 analyses). This corresponds to a composition of $Zr_{0.987}Hf_{0.013}[SiO_4]$. Lead was present in low concentrations in some analyses, but was mostly below the detection limit. In runs with baddeleyite, grains of natural baddeleyite from Phalaborwa (Hiemstra, 1955) were used.

2.2. Estimation of pressure in the HDAC

The density of the fluid loaded in the HDAC was determined from the temperature of vapor–liquid homogenization. The pressure at a given temperature and density was calculated using the equation of state (EOS) of H_2O (Wagner and Pruss, 2002). Pressure in runs with NaOH solutions was estimated using the equation of state for H_2O–NaCl (Driesner, 2007) and assuming that 1 wt% of NaOH is equivalent to 1 wt% of NaCl. For H_2O–HCl, correlation functions by Schmidt et al. (2007) were used. At high density, where no vapor bubble nucleated, the melting temperature of ice I was used to determine the fluid density. In runs with added Na_2O–SiO_2 ± Al_2O_3 glass, pressure was also estimated using the density determined from the homogenization temperature of H_2O vapor and liquid using the EOS of pure H_2O. The assumption that the EOS of pure H_2O approximates that of glass + H_2O solutions will become increasingly inaccurate as solute concentrations increase. In a parallel study, Schmidt et al. (in press) used pressure dependent shifts in the Raman bands of zircon to show that deviation from the pure H_2O EOS becomes substantial at NS3 contents greater than 30 wt% and/or at high fluid densities. However, only limited data were obtained in the NS3-H_2O system, so a rigorous pressure correction could not be derived. In contrast, only minor deviation from the pressure estimated from the pure-H_2O EOS was observed in the system $NaAlSiO_8$–H_2O (Schmidt et al., in press). This is supported in the present study by one run with 6 wt% albite, in which the pressure of 1460 MPa determined by ice VI melting temperature closely agreed with the pressure of 1390 MPa determined by the frequency shift of the ν_3 (SiO_4) Raman band of zircon (cf. Table 1). Overall, we estimate the accuracy of the pressure in this study to be about ± 50 MPa. For the runs with 30 wt% NS3, underestimation of 100–200 MPa is expected at the highest temperature and pressure investigated here.

2.3. Acquisition of X-ray fluorescence spectra

X-ray fluorescence (XRF) spectra for the determination of Zr contents were collected at a fixed energy of ca. 21 keV at beamline L, at the DORIS III storage ring of DESY, Hamburg. A high-bandwidth Ni–C multi-layer monochromator was used. The XRF spectra were collected using a confocal setup, which uses a single-bounce capillary to focus the incoming beam to ca. 10 μm and a long-distance polycapillary half-lens in front of a Si-drift detector (cf. Wilke et al., 2010). Spectra with counting times of 500 or 1000 s were taken until steady state of the Zr fluorescence intensity was reached. The intensity of the XRF signal was calibrated by measuring standard solutions containing 1000 ppm Zr with a 7 wt% HCl matrix loaded into the HDAC. The exact concentration of the standard solution after loading into the HDAC was determined by cryometry (cf. Schmidt et al., 2006).

Table 1
Zirconium concentrations and experimental conditions of solubility measurements.

Temperature (°C)	Pressure (Mpa)	Zr content (ppm)	Error* (ppm)	Glass content (wt%)	NaOH content (wt%)	Vapor–liquid homogen. temperature (°C)
Zircon in aqueous solution with $Na_2Si_3O_7$ (NS3)						
500	430	21+	1	10		219.5
550	510	25+	1	10		217
600	600	28	1	10		213
650	670	28	1	10		213
750	840	36	2	10		207
550	400	86	2	10		258.5
650	540	58	2	10		252
750	700	54	1	10		241.5
550	430	562	7	18		244.5
600	500	463	5	18		244.5
650	590	365	3	18		236.5
700	670	334	6	18		233.5
750	770	332	4	18		225
500	540	228	5	18		181.7
550	620	191	5	18		181.7
650	780	192	5	18		182.2
750	880	274	7	18		195.7
500	520	245	3	30		189
600	680	264	3	30		189
650	760	290	1	30		189
600	440	997	6	30		261
Zircon in aqueous solution with $Na_2Si_3O_7$ + 5 wt% Al_2O_3 (NS3Al5)						
660	780	112	3	20		186
700	840	108	4	20		187
750	920	125	4	20		185.5
Zircon in aqueous solution with $Na_2Si_2O_5$ (NS2)						
500	320	116	2	16		260
500	480	35	1	16		204
600	370	114	3	16		286
600	450	77	2	16		260
600	640	30	0.5	16		200
700	570	69	1	16		260
700	810	31	1	16		194
800	920	51	1	16		204
Zircon in aqueous solution with $NaAlSi_3O_8$ (albite)						
600	1460[b]	1	0.2	6		−11.5[a]
600	1460[b]	0.5	0.2	6		−11.5[a]
700	1680	0.1	0.1	6		−11.5[a]
800	1210	3	0.3	23		131
Baddeleyite in aqueous solution with NaOH						
500	540[c]	166	2		24	216
600	930[c]	359	2		24	172
300	60[c]	32	1		22	264.5
400	210[c]	34	1		22	264.5
500	370[c]	88	2		22	264.5
500	110[c]	51	0.2		21	395
600	210[c]	116	2		21	390
700	350[c]	231	2		21	375

*One standard deviation.
+Quartz present.
[a] Ice melting, no vapor bubble.
[b] 1390 MPa by Raman spectroscopy on ν_3 band of zircon.
[c] Estimated using H_2O + NaCl assuming 1 wt% NaOH = 1 wt% NaCl.

Net fluorescence intensities were corrected for density, absorption in the fluid and normalized to the intensity of the incoming beam.

2.4. Acquisition of XANES at Zr K-edge

The Zr K-edge XANES spectra presented in this paper were recorded at the European Synchrotron Radiation Facility (ESRF, Grenoble, France) on the high-brillance X-ray absorption and X-ray emission spectroscopy undulator beamline at ID26. XANES

spectra were collected in fluorescence mode using a wavelength dispersive crystal emission spectrometer (Glatzel and Bergmann, 2005). The optics at beamline ID26 consisted of a pair of multi-segmented bimorph mirrors for horizontal and vertical focusing. Further focusing was achieved by a set of 16 compound refractive lenses made of Be positioned 11.4 m upstream of the sample. The energy of the incident radiation was tuned using a pair of liquid N_2-cooled Si crystals with (311) or (111) orientation. The incident flux on the sample was monitored by detecting the X-ray scattering from a thin Kapton® foil. Spectra were recorded in a continuous quick scan mode of both monochromator and undulator gap over the energy range. The spot size of the incident X-ray beam on the sample was $80 \times 120\ \mu m^2$. High-resolution emission detection was achieved by employing 4 spherically bent Ge crystals (bending radius 1004 mm) with a (888) orientation in Rowland geometry. A Si drift detector was used for detection. During XANES scans the emission spectrometer was tuned to the $K_{\alpha 1}$ emission line of Zr (15775.1 eV). The convoluted resolution of the monochromator in the incident beam and the emission spectrometer was 2.1 eV for the Si(311) and 2.8 eV for the Si(111) monochromator.

2.5. Calculation of XANES spectra

Theoretical spectra were modeled using the FEFF code version 9.03 (Rehr and Albers, 2000; Rehr et al., 2008), which is based on a real-space multiple scattering formalism using muffin-tin potentials. Hedin–Lundqvist potentials were used for all calculations that were overlapped using the self-consistent field refinement loop. Cluster radii of 4–4.5 Å were usually sufficient. Full multiple scattering calculations were performed up to cluster radii of 6 Å for the crystalline model compounds. In order to mimic the reduced broadening of the XANES collected in the partial fluorescence yield mode the energy broadening of the calculated spectra was decreased by setting the parameter for the imaginary potential to -2 for spectra of model compounds, which were measured with the Si(311) monochromator. This parameter was set to -1 for spectra of the fluids, which were measured with the Si(111) monochromator. Quadrupolar transitions have been included for all calculations shown. Spectra were only simulated based on single clusters and thermally induced disorder was not considered.

3. Results

3.1. Zirconium concentrations in fluids

Zircon dissolved congruently in all fluids investigated. Quartz became saturated during heating in some NS3 runs at temperatures ≤ 550 °C (Table 1); however, quartz was never observed in NS2 runs. Reaction of zircon to zircono-silicates was not observed, indicating that sodium concentrations are still too low to be in their stability field even in runs with 16 wt% NS2 (Maurice, 1949). Thus, zircon + fluid ± quartz or baddeleyite + fluid is inferred to be the stable phase assemblage in the experiments. This is supported by parallel experiments with zircon and sodium silicate-bearing fluids carried out at lower silica concentrations, which did not show any sign of formation of other zirconium-bearing phases (Schmidt et al., in press; Steele-MacInnis, pers. comm.). During all runs, the evolution of the Zr concentration in the fluid was monitored by a time series of XRF measurements. Steady state was usually reached after 15–30 min. All reported concentrations represent values after reaching steady state, which was taken as the criterion for equilibration.

Table 1 summarizes the fluid composition, the experimental conditions and the Zr concentrations in equilibrium with zircon or baddeleyite of the experimental runs. Significant amounts of Zr were detected in the fluid at pressure and temperature in all runs with aqueous fluids containing NS3 component (Table 1; Fig. 1). The Zr concentration in zircon-saturated fluids with 10 wt% NS3 ranges from 21 to 86 ppm at pressures between 430 and 840 MPa and temperatures between 500 °C and 750 °C (Fig. 1a). The Zr content decreases with increasing pressure at constant temperature, as indicated by values at different pressures at 550, 650, and 750 °C (Fig. 1a). This pressure effect diminishes with increasing temperature: data at 550 °C indicate an isothermal change in concentration with pressure of -0.55 ppm/MPa, whereas at 750 °C it is -0.13 ppm/MPa.

The Zr content increases with increasing NS3 concentration (Table 1; Fig. 1b and c). For example, at 650 °C and 670–780 MPa, zircon-saturated Zr concentrations are 28, 192, and 290 ppm at NS3 contents of 10, 18, and 30 wt%, respectively. The Zr concentrations at 18 and 30 wt% NS3 show similar dependence on pressure and temperature as at 10 wt% NS3 (Fig. 1b and c).

For 10 and 18 wt% NS3, the high-pressure data define roughly linear trends that reflect data collection along the isochoric cooling path of the cell (Fig. 1a and b). The Zr concentrations along these isochores are nearly constant at 25 ppm for 10 wt% NS3 and 200 ppm for 18 wt% NS3, suggesting that Zr isopleths are roughly linear and similar in slope to isochores. This observation was used to manually estimate the linear Zr concentration contours shown in the figures.

Varying the fluid composition assessed the relative roles of Na/Si ratio and Al. Zircon solubility in 16 wt% NS2 solutions exhibits similar isothermal decrease with rising pressure (Fig. 1d). However, the Zr content is generally lower than for comparable NS3-bearing runs; e.g., 78 ppm at 600 °C, 450 MPa, in 16 wt% NS2 is ca. six times lower than in 18 wt% NS3 at 600 °C, 500 MPa (Table 1). When 5 wt% aluminum oxide was added to the NS3 composition, the Zr concentration decreased in comparison to Al-free runs with similar NS3 content. For example, dissolved Zr was lower by a factor of ca. 1.7 at 660 °C, 780 MPa, in 20 wt% NS3Al5 relative to the 18 wt% NS3 solution at the same pressure and 650 °C (Fig. 1c). Further addition of alumina to yield a metaluminous composition yielded further decrease in the Zr concentration. At 6 wt% dissolved $NaAlSi_3O_8$, the Zr concentration in the fluid is only about 1 ppm or less at pressures greater than 1460 MPa at 600–700 °C (Fig. 1e). These values are at the approximate detection limit of the method. However, they are probably not an artefact, because they are supported by the measurements at 26 wt% $NaAlSi_3O_8$, where Zr concentration is about 3 ppm at 800 °C and 1210 MPa.

To study the effects of alkalinity and pH separately, we measured Zr concentrations in NaOH solutions for comparison. Zircon is not stable in NaOH solution and would dissolve incongruently to baddeleyite (Maurice, 1949). Therefore, Zr concentrations were measured in equilibrium with natural baddeleyite. The Zr concentrations range from 32 ppm at 300 °C and 60 MPa to more than 359 ppm at 600 °C and 740–930 MPa (Fig. 1f). In this case, the Zr content increases with both pressure and temperature in contrast to fluids containing sodium-silicate components. Similar to the plots for NS3-bearing fluids and assuming linearity, the Zr concentrations are used to estimate approximate positions of Zr isopleths on the pressure–temperature diagram for the NaOH solutions.

3.2. Zr XANES spectra of model compounds

Fig. 2 shows the Zr K-edge XANES acquired for a number of model compounds with Zr in 6-, 7-, and 8-fold coordination by oxygen. Spectra on model compounds were collected at

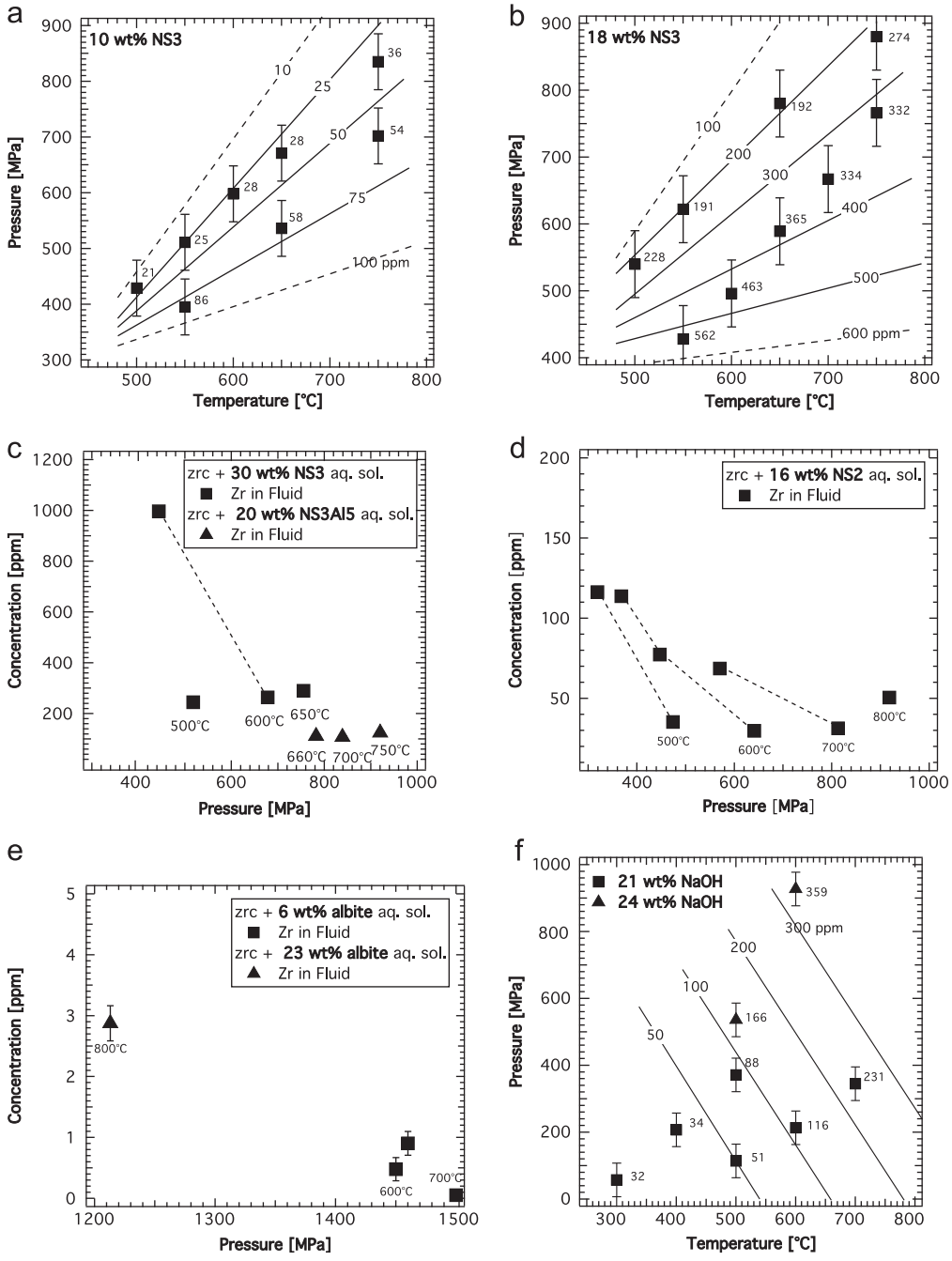

Fig. 1. Zirconium concentrations determined in-situ at high pressure and temperature. (a) Pressure–temperature diagram of zirconium concentrations for runs with 10 wt% $Na_2Si_3O_7$. Tags on data points indicate Zr concentrations. Solid and dashed lines outline estimated isopleths of Zr concentrations as indicated. (b) Pressure–temperature diagram of zirconium concentrations for runs with 18 wt% $Na_2Si_3O_7$. Tags and lines as for a. (c) Zr concentration plotted vs. pressure for runs with zircon and H_2O with 30 wt% dissolved $Na_2Si_3O_7$ and with 20 wt% dissolved $Na_2Si_3O_7$ containing 5 wt% Al_2O_3. Dashed line connects isothermal runs. (d) Zr concentration for runs with zircon and H_2O with 16 wt% dissolved $Na_2Si_2O_5$. Dashed lines connect isothermal runs. (e) runs for zircon with H_2O and dissolved $NaAlSi_3O_8$ as indicated. (f) Pressure–temperature diagram of zirconium concentrations for runs of baddeleyite with NaOH solution as indicated. Tags and lines are as for Fig. 1a.

high-energy resolution of the incident beam using a Si (311) monochromator. Armstrongite ($CaZrSi_6O_{15}\cdot 3H_2O$, Kabalov et al., 2000), elpidite ($Na_2ZrSi_6O_{15}\cdot 3H_2O$, Cannillo et al., 1973), eudialyte ($Na_{12}Ca_6Fe_3Zr_3Si_{24}O_{66}(OH)_5Cl$, Golyshov et al., 1972), and wadeite ($K_2ZrSi_3O_9$, Blinov et al., 1972) represent examples of alkali and alkaline-earth zircono-silicate minerals with Zr in 6-fold coordination. Zirconium is 8-coordinated in $ZrOCl_2\cdot 8H_2O$, zircon, and the standard solution (5000 ppm Zr) (Mak, 1968; Finger, 1974; Kanazhevskii et al., 2006; Hagfeldt et al., 2004). Seven-fold coordinated Zr is found in monoclinic ZrO_2 (baddeleyite, Smith and Newkirk, 1965). The XANES spectra are very sensitive to the local structural environment of Zr. All four alkali and alkaline-earth zircono-silicate minerals display two major peaks at the maximum of the main edge, with the weaker peak at ca. 18,018–18,020 eV, and the stronger peak at 18,032 eV. The zircon spectrum also shows a double peak at the main maximum; however, the stronger peak is at 18,020 eV whereas the weaker peak is at 18032 eV. The spectrum of monoclinic ZrO_2 exhibits only a very broad maximum at the main edge at around 18,020 eV. $ZrOCl_2\cdot 8H_2O$ displays also a broad maximum at the main edge, however, distinct from ZrO_2. Finally, the spectrum of the standard solution containing 5000 ppm of Zr is quite similar

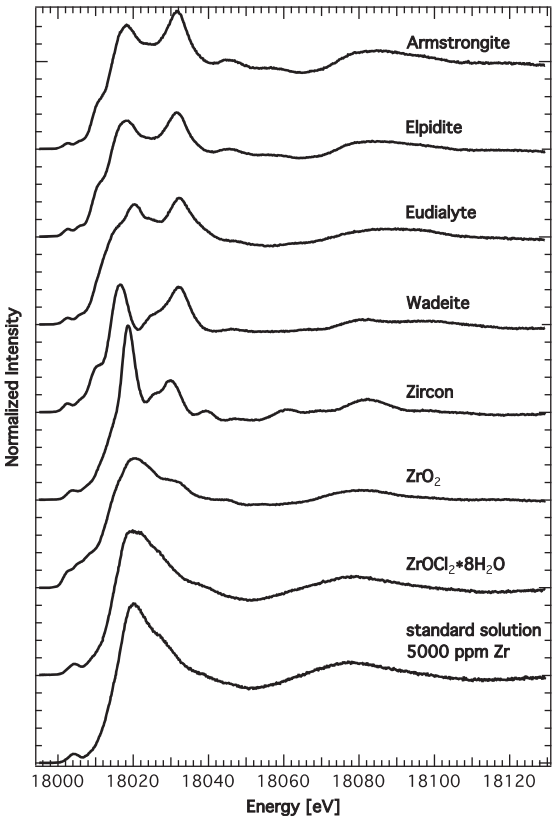

Fig. 2. Normalized Zr K-edge XANES spectra measured on model compounds in fluorescence mode using the high-resolution wavelength dispersive spectrometer in Rowland geometry. Spectra were collected in grazing-exit geometry to minimize self-absorption effects (Tröger et al., 1992). See text for further details.

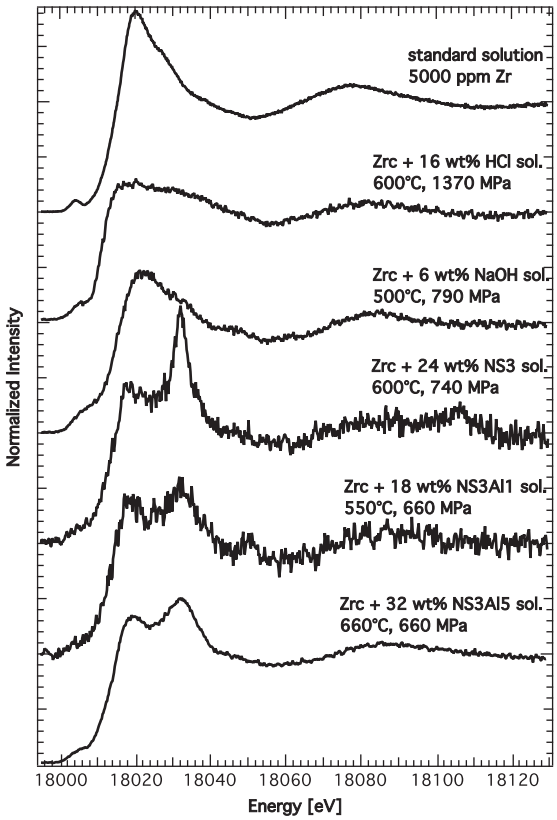

Fig. 3. Normalized Zr K-edge XANES spectra acquired in-situ on aqueous fluids at high pressure and temperature in equilibrium with zircon as indicated. The spectrum of Zr in the standard solution at ambient conditions is shown for comparison. Spectra were measured in fluorescence mode using a high-resolution wavelength dispersive spectrometer in Rowland geometry.

to that of $ZrOCl_2 \cdot 8H_2O$ except the main peak is narrower. All displayed model compounds show significant intensity in the pre-edge region (18,004–18,008 eV).

Features at the main edge mainly represent excitations of the 1s electron to unoccupied 5p states, whereas the pre-edge can be assigned to 1s→4d transitions, which are dipole-forbidden for centro-symmetric sites such as an octahedron (e.g. Li et al., 1993). Strong intensity of the pre-edge indicates substantial distortion of the coordination polyhedron from centro-symmetry and mixing of Zr d-states with the p-states of the oxygen ligands, which transfers p-character to the d-states. This assignment is consistent with the fact that all of the displayed model compounds exhibit either distorted octahedral coordination, 7-fold or non-centrosymmetric 8-fold coordination for Zr. As exemplified by the spectra of $ZrOCl_2 \cdot 8H_2O$ and the standard solution the pre-edge is strongest for the non-centrosymmetric site with the highest coordination.

3.3. Zr XANES spectra of fluids

In order to gain insight into how zircon solubility is influenced by Zr complexation in the fluid, representative XANES spectra were collected on fluid compositions similar to those that had been used to study zircon solubility. Fig. 3 shows XANES spectra for Zr in fluids equilibrated with zircon for 16 wt% HCl solution, 6 wt% NaOH solution, 24 wt% NS3 solution, 18 wt% NS3Al1 solution, and 32 wt% NS3Al5 solution. In contrast to model compounds, these spectra were acquired at lower energy resolution of the incident beam using the Si(111) monochromator (except standard solution). To the extent possible, all spectra were collected, at similar pressure and temperature in order to isolate the effect of fluid composition. Spectra acquired from the HCl and NaOH solutions clearly differ from those from NS3, NS3Al1 or NS3Al5 solutions. The spectrum taken on the HCl solution shows a very broad main maximum between 18,018 and 18,050 eV with contributions by 3 spectral features, followed by a relatively broad first maximum at ca. 18,080 eV. In the case of the NaOH solution, the main maximum at ca. 18,022 eV is significantly narrower and shows two additional features on the high-energy limb, followed by a small feature at ca. 18,060 eV. Another spectrum, not shown, was taken on a 4.7 wt% NaOH solution in equilibrium with baddeleyite at 500 °C and 530 MPa to check for potential effects on the complexation by Si from dissolution of zircon. Unfortunately, this spectrum is noisy due to low signal and insufficient integration time but it does not indicate any major difference to the one taken on zircon in NaOH solution.

In contrast, spectra taken on the fluids containing NS3, NS3Al1, or NS3Al5 differ considerably from those of the HCl and NaOH solutions. All three show a main maximum with two separate peaks at 18,020 and 18032 eV. The two Al-bearing compositions are similar, whereas the spectrum of the NS3-bearing fluid displays a significantly sharper and more intense peak at 18,032 eV. The features at 18,090 and 18,110 eV visible for the NS3-fluid and the feature at 18,050 eV for the NS3Al1 are artefacts caused by Bragg diffraction from the diamond anvils. All spectra shown display a distinct feature in the pre-edge region, although it is less pronounced compared to the model compounds due to the higher energy bandwidth of the incoming beam.

3.4. Modeling of Zr XANES spectra

3.4.1. Zirconium in model compounds

Theoretical XANES spectra were computed using the FEFF code (Rehr and Albers, 2000; Rehr et al., 2008) to help constrain

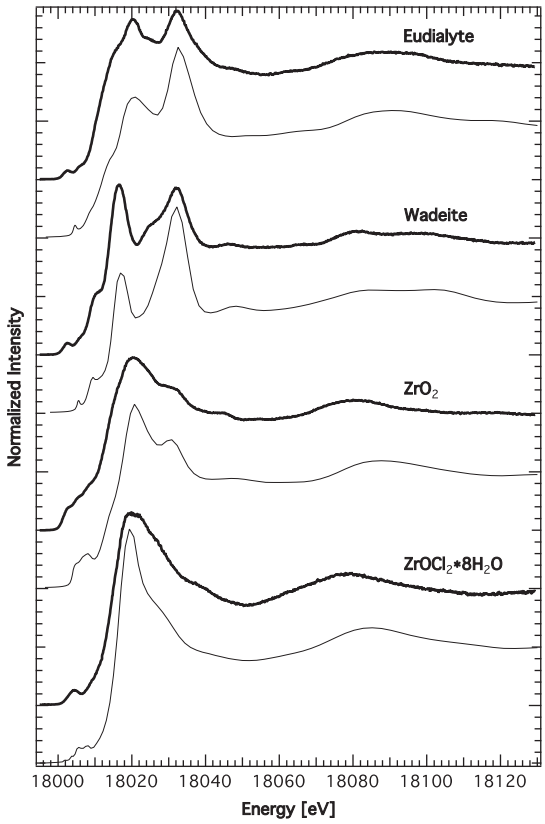

Fig. 4. Comparison of experimental (thick lines) and simulated (thin lines) XANES spectra of model compounds.

interpretations for the structural environment of Zr in the fluids. As a first step, spectra of model compounds were generated to evaluate the agreement between the calculated and experimentally observed features. Fig. 4 compares calculated and experimental XANES spectra for a selection of model compounds. Calculated spectra agree very well with experimental spectra (Fig. 4). Calculated spectra clearly show a well-separated pre-edge feature that indicates contribution from quadrupolar transitions, which was evaluated by comparing calculations with and without quadrupolar transitions. Calculations including quadrupolar transitions show a distinctively enhanced pre-edge feature, that matches better the experimental spectra. Some of the mismatch observed between experiment and calculation might be related to approximations used by the FEFF code, such as the muffin-tin potential as well as the treatment of the core–hole, which can have significant effects in the XANES region (e.g. Rehr and Albers, 2000). Alternatively, there could be differences between the crystal structures used as input and the real structures of the studied samples.

3.4.2. *Zirconium in fluids*

Theoretical spectra of Zr in the aqueous fluids were calculated using small clusters as input structures, guided by comparison of the fluid spectra with those of model compounds. For Zr in the standard solution, simulation of a spectrum based on a ZrO_8-cluster as found in $ZrOCl_2 \cdot 8H_2O$ agrees very well with the experiment (Fig. 5a). It reproduces the pre-edge feature as well as the fine structure at the main edge with a very good match in the relative energy positions compared to the experiment. In this ZrO_8-cluster, the oxygen ligands form an irregular polyhedron with Zr–O distances ranging from 2.110 to 2.338 Å (Mak, 1968),

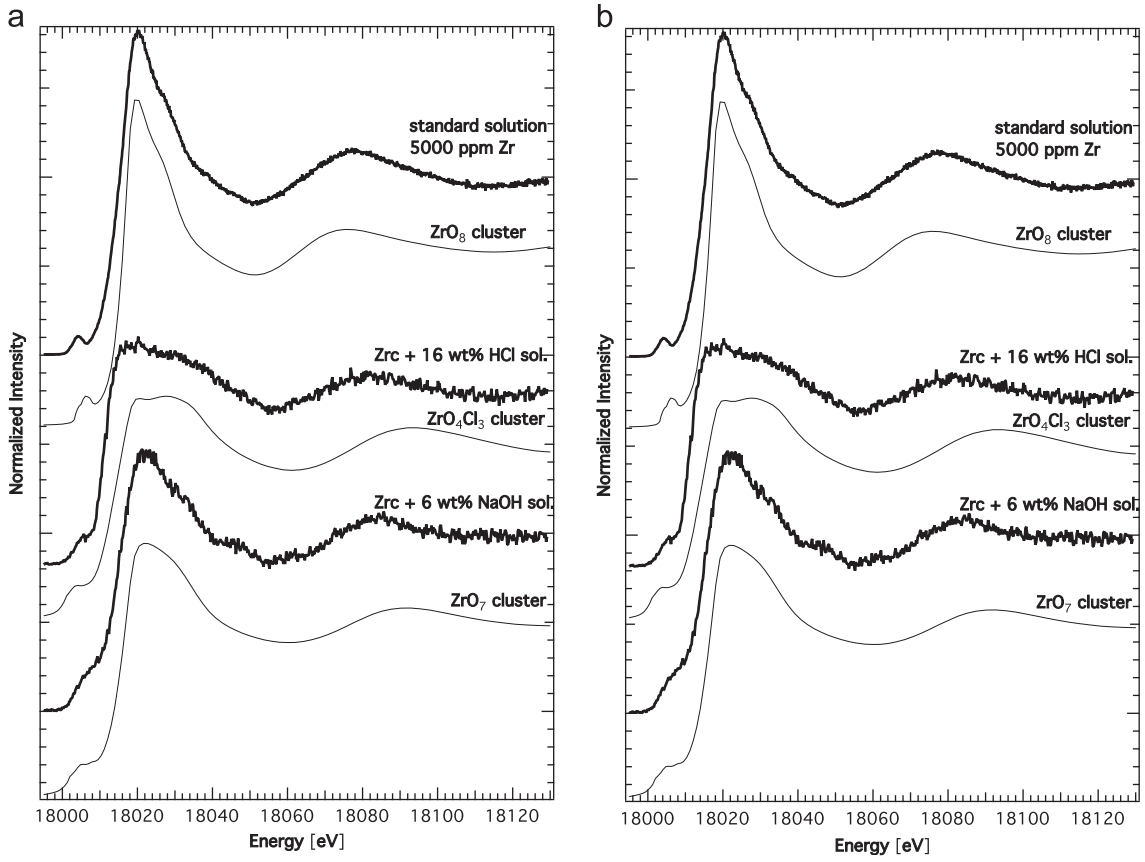

Fig. 5. Comparison of experimental (thick lines) and simulated (thin lines) XANES spectra for Zr in aqueous fluids. (a) spectra of Zr in basic and acidic solutions. (b) spectra of Zr in aqueous fluids with Na–Al–Si components as indicated. Spectra shown here are the same as shown in Fig. 3, where experimental conditions are indicated.

which is consistent with the results of Hagfeldt et al. (2004) and Kanazhevskii et al. (2006).

For the NaOH solution, a spectrum calculated based on a ZrO_7-cluster similar to monoclinic ZrO_2 with Zr–O distances of 2.051–2.285 Å (Smith and Newkirk, 1965) most closely resembles the experiment (Fig. 5a). This includes an enhanced pre-edge and the fine structure at the main maximum. The feature at ca. 18,045 eV, missing in the calculated spectrum, may indicate contributions by higher coordination shells, which were not considered in the calculation. Possibly it may stem from Zr via the presence of oligomeric zirconyl units or from Na due to Zr–Na complexing.

The spectrum of the HCl-solution equilibrated with zircon does not resemble any of the model compounds. In order to evaluate whether some of the oxygen ligands are replaced by chlorine, spectra were calculated for $ZrCl_x$ as well as for ZrO_x clusters where part of the oxygens were replaced by Cl. The only spectrum that yielded a reasonable match is based on a ZrO_4Cl_3-cluster (Fig. 5a), and was produced by replacing the outermost oxygen atoms of the ZrO_7-cluster of ZrO_2 by chlorine. This results in 4 oxygen neighbors with distances between 2.051 and 2.163 Å and 3 chlorine atoms at distances between 2.189 and 2.284 Å.

The best match for the spectra with dissolved silicate components was obtained using clusters derived from the sodium zircono-silicates vlasovite ($Na_2ZrSi_4O_{11}$, Voronkov et al., 1974; Gobechiya et al., 2003) and catapleite ($Na_2ZrSi_3O_9 \cdot 2H_2O$, Ilyushin et al., 1981). In both compounds, Zr is in distorted octahedral coordination. In vlasovite two oxygen atoms are found at distances of 2.062 Å, 2.093 Å and 2.116 Å (Gobechiya et al., 2003), whereas for catapleite two oxygen atoms are at 2.066 and four at 2.079 Å (Ilyushin et al., 1981). In all cases the peak at ca. 18,032 eV is reproduced well (Fig. 5b). The calculations reproduce the pre-edge region reasonably well, where the spectra based on the catapleite cluster show higher intensity more similar to the experiment and indicate a considerable distortion from octahedral symmetry for the ZrO_6 complex in the fluid. The peak at ca. 18,020 eV is only reproduced if higher coordination shells are included (Fig. 5b, $R=4.0$ Å), which is a strong evidence for complexing of Zr with Si and Na in these fluids. Although the calculated spectra based on vlasovite and catapleite do not fully match the experiment and cannot resolve the slight differences between different fluid compositions, they provide a strong constraint for the octahedral coordination by oxygen, and complexing of ZrO_6 with dissolved silicate components.

4. Discussion

4.1. Zircon and baddeleyite solubility in H_2O

Over a wide range of crustal and mantle conditions, zircon dissolves incongruently in pure H_2O via the reaction: zircon = baddeleyite + SiO_2 (aq.). Incongruent dissolution arises from much lower solubility of Zr relative to Si (Newton et al., 2005, 2010). Tole (1985) estimated the Zr content in water coexisting with zircon to be far below 0.05 ppm for temperatures up to 80 °C at ambient pressure. Newton et al. (2005, 2010) were unable to determine the Zr concentrations in Si-bearing H_2O equilibrated with zircon + baddeleyite at 800 °C and 1.2 GPa. Ayers and Watson (1991) reported zircon solubilities in pure H_2O at 1–2 GPa, 1000–1100 °C of up to 6.9 wt%; however, their methods led to significant overestimation of solubility (Tropper and Manning, 2005; Antignano and Manning, 2008). To our knowledge, there are no further data on Zr-contents in pure H_2O at metamorphic conditions. This is surely because Zr concentrations in the fluid are very low and difficult to determine. The analytical procedure used here does not allow measurement of the zircon solubility in pure water because the detection limit of this setup here (ca. 1 ppm, see Wilke et al., 2010) would still need to be about 100 times better.

At a given pressure and temperature, acidic or alkaline solutions should lead to higher zircon solubility, provided that both positively and negatively charged $Zr(OH)_n^{4-n}$ species are stable (e.g., Adair et al., 1997). At 400 °C, 90 MPa, and $ZrO_2/SiO_2=1$, Maurice (1949) found zircon to stably coexist with acidic solutions, whereas in basic solutions baddeleyite and zircono-silicates were found to be stable, suggesting incongruent dissolution is favoured by elevated pH. Schmidt et al. (2006) found congruent dissolution behavior and significant Zr solubility in HCl solutions equilibrated with crystalline zircon. Zircon solubility increased with HCl-content and temperature. For example, Zr concentrations reached more than 9000 ppm at 500 °C and 290 MPa in 7.9 m HCl solution. Ewing et al. (1982) provide data on Zr-contents for partially metamict natural zircon equilibrated with basic solutions at low pressure of ca. 2 atm and 87 °C, which show Zr-contents between 0.027 and 12.79 ppm depending on the degree of metamictization or alpha dose.

To facilitate comparison with Na–Si–Al fluids, we focused on determination of Zr concentrations in basic NaOH solutions. Baddeleyite was used instead of zircon because of previously reported incongruent dissolution of zircon. Baddeleyite solubility in 21–24 wt% NaOH is 32–359 ppm at 500–700 °C and 320–930 MPa, well above detection limits and higher than for baddeleyite in pure H_2O (Newton et al., 2010). In addition, baddeleyite solubility in NaOH increases isobarically with rising temperature as well as with isothermal increase in pressure. These results are consistent with the expected amphoteric behavior of zirconium hydroxide complexes; however, it is possible that elevation of baddeleyite solubility in NaOH arises in part from Na-zirconium hydroxide complexing similar to observations by Brendebach et al. (2007) for Zr in basic calcium chloride solutions.

4.2. Zircon solubility in H_2O-rich crustal and mantle fluids

Fluids such as pure H_2O, H_2O–HCl, or H_2O–NaOH are not realistic approximations of those that would be found at metamorphic conditions in the crust or mantle. This is because strong interactions of any of these fluids with the adjacent rock matrix would result in considerable dissolution of major rock-forming components into the fluid. At high pressure and temperature, metamorphic fluids will contain substantial silica, alumina and alkalis (e.g., Manning, 1994; Manning et al., 2010; Wohlers et al., 2011). Though zircon solubility in such fluids has not previously been determined, elevated solubility might be expected because Watson (1979) and Watson and Harrison (1983) report significant zircon solubility in hydrous silicate melts at 200 MPa and 700–1080 °C, with a strong positive correlation of the zircon saturation with the alkali/Al of the melts.

We find that, compared to Zr concentrations expected for pure water, the Zr-contents measured for fluids containing NS3, NS3Al5 and albite components all represent a strong enhancement of the Zr concentration for fluids in equilibrium with zircon. The Zr concentrations generally exhibit isobaric increase with temperature and with the amount of components dissolved, whereas they decrease with increase in isothermal pressure. Increase of the Na/Si of the fluid as well as addition of Al lowers the Zr contents at constant pressure and temperature.

Our observations for zircon are consistent with results determined on the solubility of rutile in similar fluid compositions (Manning et al., 2008; Antignano and Manning, 2008), although the Zr concentrations are lower by a factor of 3 to 5 compared to Ti contents at comparable conditions. Hayden and Manning (2011) also observed that rutile solubility in ≥ 30 wt% albite solutions decreased with increasing pressure at constant temperature. The concentrations

reached in the fluid are in the same order of magnitude as those attained in NaOH solutions or in HCl solutions (Schmidt et al., 2006) at comparable pressure and temperature.

4.3. Origin of zircon solubility enhancement

Any enhancement of Zr-contents by change of the fluid composition points to considerable changes in the complexation of Zr in the fluid. Addition of NaOH will favor formation of hydroxyl-bearing complexes, whereas HCl-bearing fluids will stabilize chloride or oxychloride complexes (e.g. Maurice, 1949; Aja et al., 1995). Similarly, the enhancement produced by adding NS3 or albite component to the fluid implies formation of Zr complexes that are energetically more favorable than those in pure H_2O. Although Zr contents are of the same order of magnitude as those measured for the NaOH solution and addition of NS3 will produce an alkaline solution, the mechanism of Zr complexation is likely to be different for these two compositions. This is already evident by the completely different dependence of the Zr concentration on pressure and temperature (cf. Fig. 1a–f), where a strong isothermal decrease with pressure is observed for NS3-bearing fluids and an increase with pressure for NaOH solutions.

Manning et al. (2008) and Antignano and Manning (2008) suggested the formation of alkali-titanate complexes in the fluid as postulated for Ti in silicate melts (Dickenson and Hess, 1985) to explain the high rutile solubility in silicate-bearing fluids. The inverse correlation of Ti and Al contents was taken as evidence for competition for Na between Na–Al–Si polymers and alkali-titanate complexes.

Similar arguments may be used to derive a complexation mechanism for Zr in the silicate-bearing fluids. Zircon solubility data in silicate melts and the strong influence of the alkali–aluminum ratio on the Zr concentration in the melt led Watson (1979) to postulate the presence of Zr melt-species similar to the local structure of Zr in alkali zircono-silicates, e.g. $Na_4Zr(SiO_4)_2$. Farges et al. (1991) provided spectroscopic evidence that these units may be present in peralkaline silicate melts leading to 6-fold coordinated Zr, whereas the incorporation mechanism is different for metaluminous compositions, where 8-fold coordinated Zr is found.

If zircono-silicate complexes were present in these fluids the inverse correlation of Zr with Al implies that their formation is strongly influenced by the presence of Al, and that they do not incorporate Al. The strong decrease of Zr concentration with pressure in NS3-bearing fluids very likely correlates with increased silica polymerization (e.g. Zotov and Keppler, 2002) and may suggest that this leads to destabilizing the alkali zircono-silicate complexes. Interestingly, Aja et al. (1995) reported relatively high Zr concentrations for solubility experiments of the zircono-silicate vlasovite, which may be taken as further evidence for the formation of alkali zircono-silicate complexes in the fluid.

Analysis of the XANES spectra taken on the fluids at pressure and temperature provides a first order estimate for the Zr coordination in the fluids and their relation to the fluid composition. Eight-fold coordinated Zr is found in the standard solution containing 5000 ppm Zr. The spectrum for Zr in HCl-solution in equilibrium with zircon can be assigned to a coordination environment containing both chloride and oxygen as ligands at a total coordination number of 7. The spectrum of Zr in the NaOH-solution in equilibrium with baddeleyite is reasonably well reproduced by 7-fold coordinated Zr. The spectra of fluids with NS3 and NS3Al5/NS3Al1 are indicative of $^{[6]}$Zr. Among models derived from alkali zircono-silicates, the model with the best match is obtained for clusters based on vlasovite or catapleite. A considerable improvement of the simulation is obtained if higher coordination shells are included. The inclusion of Si and Na next-nearest neighbors is particularly important to reproduce the characteristic doublet at the main edge. This provides strong evidence for the presence of Zr in polymeric silicate units, and suggests that the enhancement of zircon solubility in these fluids is due to complexation of Zr in units closely resembling the local structure around Zr in alkali zircono-silicates. Therefore, the XANES spectra strongly support the idea of formation of alkali zircono-silicate complexes in these fluids as derived from solubility data. Polymerization of Zr in solutions seems to be a fundamental incorporation mechanism of Zr, as evidenced in several studies on Zr in synthetic solutions particularly at high concentrations (e.g. Zielen and Connick, 1956; Kanazhevskii et al., 2001, 2006; Hagfeldt et al., 2004; Cho et al., 2005). Brendebach et al. (2007) identified Ca–Zr-OH complexes with $^{[6]}$Zr for basic $CaCl_2$ solutions, which showed high solubility for hydrous zirconium oxide. In this case, association with Ca stabilizes the relatively high number of OH^--ligands around Zr. Thus, the higher coordination number that can be reached by clustering of Zr or polymerization with other components seems to be energetically more favorable over the formation Zr monomers in pure H_2O.

5. Conclusions

The solubility of zircon is strongly enhanced in aqueous fluids containing $Na_2Si_3O_7$ or $Na_2Si_2O_5$ components. Addition of alumina decreases the Zr concentration in the fluid, so that the solubility is less enhanced for $H_2O+NaAlSi_3O_8$. The similarity to results on Ti (Manning et al., 2008; Antignano and Manning, 2008) suggests that this effect can be generalized to all HFSE. The investigations by XANES spectroscopy strongly support the hypothesis derived from the solubility data that formation of alkali zircono-silicate complexes may be responsible for the enhancement of zircon solubility in Na–Al–Si-bearing fluids.

The results of this study imply that interactions between fluid and rock matrix will have a strong effect on the capability of the fluid in mobilizing Zr or HFSE in general. For example, incongruent dissolution of feldspar and mica at high pressure and temperature will probably result in an alkali/Al greater than unity in aqueous fluids, for which our data suggest substantial concentrations of Zr or HFSE. This hypothesis is further supported by the observed significant positive correlation between signs of zircon recrystallization and abundance of phyllosilicates in low-grade metamorphosed sediments (Hay and Dempster, 2009). On the other hand, any change in the surrounding lithology during migration of fluids will change the composition of the dissolved silicate fraction and thus will also influence the capability of transporting HFSE. Therefore, large-scale transport across lithologies buffering a low Na/Al ratio in the fluid is probably not possible.

Acknowledgments

We thank the ESRF and DESY for providing beamtime. The technical support of O. Appelt, D. Rhede, S. Gehrmann, R. Schulz (GFZ), C. Lapras (ESRF) and W. Ternes (DESY) is highly appreciated. We also thank A. Wohlers and S. Simon for helpful support during beam time and A. Snigirev for providing the set of Be lenses. This work benefited from a grant by the DFG (WI 2000/5-1). CEM was supported by National Science Foundation Grant EAR-1049901.

References

Adair, J.H., Karup, H.G., Venigalla, S., Tsukada, T., 1997. A review of the aqueous chemistry of the zirconium–water system to 200 °C. Mater. Res. Soc. Symp. Proc. 432, 101–112.

Aja, S.U., Wood, S.A., Williams-Jones, A.E., 1995. The aqueous geochemistry of Zr and the solubility of some Zr-bearing minerals. Appl. Geochem. 10, 603–620.
Antignano, A., Manning, C.E., 2008. Rutile solubility in H_2O, H_2O–SiO_2, and H_2O–$NaAlSi_3O_8$ fluids at 0.7–2.0 GPa and 700–1000 °C: implications for mobility of nominally insoluble elements. Chem. Geol. 255, 283–293.
Audétat, A., Keppler, H., 2005. Solubility of rutile in subduction zone fluids, as determined by experiments in the hydrothermal diamond anvil cell. Earth Planet. Sci. Lett. 232, 393–402.
Ayers, J.C., Watson, E.B., 1991. Solubility of apatite, monazite, zircon, and rutile in supercritical aqueous fluids with implications for subduction zone geochemistry. Philos. Trans. R. Soc. London A 335, 365–375.
Bassett, W.A., Shen, A.H., Bucknum, M., Chou, I-M., 1993. A new diamond anvil cell for hydrothermal studies to 2.5 GPa and from −190 to 1200 °C. Rev. Sci. Instrum. 64, 2340–2345.
Blinov, V.A., Shumyatskayo, N.G., Voronkov, A.A., Ilyuskin, V.V., Belov, N.V., 1972. Refinement of the crystal structure of wadeite $K_2Zr(Si_3O_9)$ and its relation to kindred structural types. Kristallographiya 17, 1119–1123.
Borchert, M., Wilke, M., Schmidt, C., Rickers-Appel, K., 2009. Partitioning and equilibration of Rb and Sr between silicate melts and aqueous fluids. Chem. Geol. 259, 39–47.
Brenan, J.M., Shaw, H.F., Phinney, D.L., Ryerson, F.J., 1994. Rutile-aqueous fluid partitioning of Nb, Ta, Hf, Zr, U and Th: implications for high field strength element depletions in island-arc basalts. Earth Planet. Sci. Lett. 128, 327–339.
Brendebach, B., Altmaier, M., Rothe, J., Neck, V., Denecke, M.A., 2007. EXAFS study of aqueous Zr^{IV} and Th^{IV} complexes in alkaline $CaCl_2$ solutions: $Ca_3[Zr(OH)_6]^{4+}$ and $Ca_4[Th(OH)_8]^4$. Inorg. Chem. 46, 6804–6810.
Cannillo, E., Rossi, G., Ungaretti, L., 1973. The crystal structure of elpidite. Am. Mineral. 58, 106–109.
Cho, H.R., Walther, C., Rothe, C., Neck, V., Denecke, M.A., Dardenne, K., Fanghänel, T., 2005. Combined LIBD and XAFS investigation of the formation and structure of Zr(IV) colloids. Anal. Bioanal. Chem. 383, 28–40.
Dempster, T.J., Hay, D.C., Bluck, B.J., 2004. Zircon growth in slate. Geology 32, 221–224.
Dickenson Jr., J.E., Hess, P.C., 1985. Rutile solubility and titanium coordination in silicate melts. Geochim. Comsochim. Acta 49, 2289–2296.
Driesner, T., 2007. The system H_2O–NaCl. Part II: correlations for molar volume, enthalpy, and isobaric heat capacity from 0 to 1000 °C, 1 to 5000 bar, and 0 to 1 × NaCl. Geochim. Cosmochim. Acta 71, 4902–4919.
Elliott, T., Plank, T., Zindler, A., White, W., Bourdon, B., 1997. Element transport from slab to volcanic front at the Mariana arc. J. Geophys. Res.—Solid Earth 102, 14991–15019.
Ewing, R.C., Haaker, R.F., Lutze, W., 1982. Leachability of zircon as a function of alpha dose. In: Lutze, W. (Ed.), Scientific Basis for Radioactive Waste Management V. Elsevier, Amsterdam, pp. 389–397.
Farges, F., Ponader, C.W., Brown Jr., G.E., 1991. Structural environments of incompatible elements in silicate glass/melt systems: I. Zirconium at trace levels. Geochim. Cosmochim. Acta 55, 1563–1574.
Finger, L.W., 1974. Refinement of the Structure of Zircon. Carnegie Institution of Washington Yearbook, vol. 73; (pp. 544–547).
Glatzel, P., Bergmann, U., 2005. High-resolution 1s core hole X-ray spectroscopy in 3d transition metal complexes—electronic and structural information. Coord. Chem. Rev. 249, 65–95.
Gobechiya, E.R., Pekov, I.V., Pushcharovskii, D.Y., Ferraris, G., Gula, A., Zubkova, N.V., Chukanov, N.V., 2003. New data on vlasovite: refinement of the crystal structure and radiation damage of the crystal during X-ray diffraction experiment. Kristallografiya 48, 808–812.
Golyshov, V.M., Simonov, V.I., Belov, N.V., 1972. Crystal structure of eudialyte. Kristallografiya 17, 1119–1123.
Hagfeldt, C., Kessler, V., Persson, I., 2004. Structure of the hydrated, hydrolysed and solvated zirconium(IV) and hafnium(IV) ions in water and aprotic oxygen donor solvents. A crystallographic, EXAFS spectroscopic and large angle X-ray scattering study. Dalton Trans., 2142–2151.
Hay, D.C., Dempster, T.J., 2009. Zircon behavior during low-temperature metamorphism. J. Petrol. 50, 571–589.
Hayden, L.A., Manning, C.E., 2011. Rutile solubility in supercritical $NaAlSi_3O_8$–H_2O fluids. Chem. Geol. 284, 74–81.
Hiemstra, S.A., 1955. Baddeleyite from Phalaborwa, Eastern Transvaal. Am. Mineral. 40, 275–282.
Hoskin, P.W.O, Schaltegger, U., 2003. The composition of zircon and igneous and metamorphic processes. Rev. Mineral. Geochem. 53, 27–62.
Ilyushin, G.D., Voronkov, A.A., Ilyukhin, V.V., Nevskii, N.N., Belov, N.N., 1981. Crystal structure of natural monoclinic catapleite $Na_2ZrSi_3O_9 \cdot 2H_2O$. Sov. Phys. Dokl. 26, 808–810.
John, T., Klemd, R., Gao, J., Garbe-Schonberg, C.D., 2008. Trace-element mobilization in slabs due to non steady-state fluid–rock interaction: constraints from an eclogite-facies transport vein in blueschist (Tianshan, China). Lithos 103, 1–24.
Kabalov, Y.K., Zubkova, N.V., Pushcharovskii, D.Y., Schneider, J., Sapozhnikov, A.N., 2000. Powder Rietveld refinement of armstrongite, $CaZr[Si_6O_{15}] \cdot 3H_2O$. Z. Kristallogr. 125, 757–761.
Kamber, B.S., Collerson, K.D., 2000. Zr/Nb systematics of Ocean Island basalts reassessed—the case for binary mixing. J. Petrol. 41, 1007–1021.
Kanazhevskii, V.V, Novgorodov, B.B, Shmachkova, V.P., Kotsarenko, N.S, Kriventsov, V.V., Kochubey, D.I., 2001. Structure of zirconium complexes in aqueous solutions. Mendeleev Commun. 11, 211–212.
Kanazhevskii, V.V, Shmachkova, V.P., Kotsarenko, N.S, Kolomiichuk, V.N., Kochubei, D.I., 2006. J. Struct. Chem. 47, 860–868.
Li, P., Chen, I-W., Penner-Hahn, J.E., 1993. X-ray-absorption studies of zirconia polymorphs. I. Characteristic local structures. Phys. Rev. B. 48, 10063–10073.
Liati, A., Gebauer, D., 1999. Constraining prograde and retrograde P–T–t paths of Eocene HP rocks by SHRIMP dating of different zircon domains: inferred rates of heating, burial, cooling and exhumation for central Rhodope, northern Greece. Contrib. Mineral. Petrol. 135, 340–354.
Mak, T.C.W., 1968. Refinement of the crystal structure of zirconyl chloride octahydrate. Can. J. Chem. 46, 3491–3497.
Manning, C.E., 1994. The solubility of quartz in H_2O in the lower crust and upper mantle. Geochim. Cosmochim. Acta 58, 4831–4839.
Manning, C.E., Wilke, M., Schmidt, C., Cauzid, J., 2008. Rutile solubility in albite–H_2O and $Na_2Si_3O_7$–H_2O at high temperatures and pressures by in-situ synchrotron radiation micro-XRF. Earth Planet. Sci. Lett. 272, 730–737.
Manning, C.E., Antignano, A., Lin, H.A., 2010. Premelting polymerization of crustal and mantle fluids, as indicated by solubility of albite + paragonite + quartz in H_2O at 1 GPa and 350–620 °C. Earth Planet. Sci. Lett. 292, 325–336.
Maurice, O.D., 1949. Transport and deposition of the non-sulphide vein minerals. V. Zirconium minerals. Econ. Geol. 44, 721–731.
Mazurin, O.V., Streltsina, M.V., Shviko-Shvikovskaya, T.P., 1983. Handbook of Glass Data, Part A. Silica Glass and Binary Silicate Glasses. Elsevier, Amsterdam.
Mazurin, O.V., Streltsina, M.V., Shviko-Shvikovskaya, T.P., 1987. Handbook of Glass Data, Part C. Ternary Silicate Glasses. Elsevier, Amsterdam.
McCulloch, M.T., Gamble, J.A., 1991. Geochemical and geodynamical constraints on subduction zone magmatism. Earth Planet. Sci. Lett. 102, 358–374.
Möller, A., O'Brien, P.J., Kennedy, A., Kröner, A., 2002. Polyphase zircon in ultrahigh-temperature granulites (Rogaland, SW Norway): constraints for Pb diffusion in zircon. J. Metamor. Geol. 20, 727–740.
Mysen, B.O., Takahashi, K., 2010. Structure of H_2O-saturated peralkaline aluminosilicate melt and coexisting aluminosilicate-saturated aqueous fluid determined in-situ to 800 C and ~800 MPa. Geochim. Cosmochim. Acta 74, 4123–4139.
Newton, R.C., Manning, C.E., Hanchar, J.M., Finch, R.J., 2005. Gibbs free energy of formation of zircon from measurement of solubility in H_2O. J. Am. Ceram. Soc. 88, 1854–1858.
Newton, R.C., Manning, C.E., Hanchar, J.M., Colasanti, C.V., 2010. Free energy of formation of zircon based on solubility measurements at high temperature and pressure. Am. Mineral. 95, 52–58.
Perfit, M.R., Gust, D.A., Bence, A.E., Arculus, R.J., Taylor, S.R., 1980. Chemical characteristics of island-arc basalts: implications for mantle sources. Chem. Geol. 30, 227–256.
Philippot, P., Selverstone, J., 1991. Trace-element-rich brines in eclogitic veins: implications for fluid composition and transport during subduction. Contrib. Mineral. Petrol. 106, 417–430.
Rapp, J.F., Klemme, S., Butler, I.B., Harley, S.L., 2010. Extremely high solubility of rutile in chloride and fluoride-bearing metamorphic fluids: an experimental investigation. Geology 38, 323–326.
Rehr, J.J., Albers, R.C., 2000. Theoretical approaches to x-ray absorption fine structure. Rev. Mod. Phys. 72, 621–654.
Rehr, J.J., Kas, J.J., Prange, M.P., Sorini, A.P., Takimoto, Y., Vila, F., 2008. Ab initio theory and calculations of X-ray spectra. C. R. Phys. 10, 548–559.
Rudnick, R.L., Barth, M., Horn, I., McDonough, W.F., 2000. Rutile-bearing refractory eclogites: missing link between continents and depleted mantle. Science 287, 278–281.
Schmidt, C., Rickers, K., 2003. In-situ determination of mineral solubilities in fluids using a hydrothermal diamond-anvil cell and SR-XRF: solubility of AgCl in water. Am. Mineral. 88, 288–292.
Schmidt, C., Rickers, K., Wirth, R., Nasdala, L., Hanchar, J.M., 2006. Low-temperature Zr mobility: an in-situ synchrotron radiation XRF study of the effect of radiation damage in zircon on the element release in $H_2O + HCl \pm SiO_2$ fluids. Am. Mineral. 91, 1211–1215.
Schmidt, C., Rickers, K., Bilderback, D.H., Huang, R., 2007. In situ synchrotron-radiation XRF study of REE phosphate dissolution in aqueous fluids to 800 °C. Lithos 95, 87–102.
Schmidt C., Steele-MacInnis, M., Watenphul, A., Wilke, M. Calibration of zircon as a Raman spectroscopic pressure sensor to high temperatures and application to water-silicate melt systems. Am. Mineral., in press.
Smith Jr., D.K., Newkirk, H.W., 1965. The crystal structure of baddeleyite (monoclinic ZrO_2) and its relation to the polymorphism of ZrO_2. Acta Crystallogr. 18, 983–991.
Tanaka, M., Takahashi, K., 1999. The identification of chemical species of silica in sodium hydroxide, potassium hydroxide and sodium chloride solutions by FAB-MS. Anal. Sci. 15, 1241–1250.
Tole, M.P., 1985. The kinetics of dissolution of zircon ($ZrSiO_4$). Geochim. Cosmochim. Acta 49, 453–458.
Tröger, L., Arvanitis, D., Baberschke, K., Michaelis, H., Grimm, U., Zschech, E., 1992. Full correction of the self-absorption in soft-fluorescence extended X-ray absorption fine structure. Phys. Rev. B 46, 3283–3289.
Tropper, P., Manning, C.E., 2005. Very low solubility of rutile in H_2O at high pressure and temperature, and its implications for Ti mobility in subduction zones. Am. Mineral. 90, 502–505.
Van Baalen, M., 1993. Titanium mobility in metamorphic systems—a review. Chem. Geol. 110, 233–249.
Vavra, G., Gebauer, D., Schmid, R., Compston, W., 1996. Multiple zircon growth and recrystallisation during polyphase Late Carboniferous to Triassic

metamorphism in granulites of the Ivrea Zone (Southern Alps): an ion microprobe (SHRIMP) study. Contrib. Mineral. Petrol. 122, 337–358.
Voronkov, A.A., Zhdanova, T.A., Pyatenko, Y.A., 1974. Refinement of the structure of vlasovite $Na_2ZrSi_4O_{11}$ and some characteristics of the composition and structure of the zirconosilicates. Kristallografiya 19, 252–259.
Wagner, W., Pruss, A., 2002. The IAPWS formulation 1995 for the thermodynamic properties of ordinary water substance for general and scientific use. J. Phys. Chem. Ref. Data 31, 387–535.
Watson, E.B., 1979. Zircon saturation in felsic liquids: experimental results and application to trace element geochemistry. Contrib. Mineral. Petrol. 70, 407–419.
Watson, E.B., Harrison, T.M., 1983. Zircon saturation revisited: temperature and composition effects in a variety of crustal magma types. Earth Planet. Sci. Lett. 64, 295–304.
Wilke, M., Appel, K., Vincze, L., Schmidt, C., Borchert, M., Pascarelli, S., 2010. A confocal set-up for micro-XRF and XAFS experiments using diamond-anvil cells. J. Synchr. Rad. 17, 669–675.
Wohlers, A., Manning, C.E., Thompson, A.B., 2011. Experimental investigation of the solubility of albite and jadeite in H_2O, with paragonite+quartz at 500 °C and 600 °C, and 1–2.25 GPa. Geochim. Cosmochim. Acta 75, 2924–2939.
Zielen, A.J., Connick, R.E., 1956. The hydrolytic polymerization of zirconium in perchloric acid solutions. J. Am. Chem. Soc. 78, 5785–5792.
Zotov, N., Keppler, H., 2002. Silica speciation in aqueous fluids at high pressures and high temperatures. Chem. Geol. 184, 71–82.